Volume 44
Number 10
14 March 2020
Pages 3805–4230

NJC

New Journal of Chemistry

A journal for new directions in chemistry

rsc.li/njc

ISSN 1144-0546

ROYAL SOCIETY OF CHEMISTRY

PAPER

Wei Liu, Dawei Luo *et al.*

Enhanced thermal stability and wettability of an electrospun fluorinated poly(aryl ether ketone) fibrous separator for lithium-ion batteries

cnrs

NJC

ROYAL SOCIETY OF CHEMISTRY

PAPER

View Article Online
View Journal | View Issue

Cite this: *New J. Chem.*, 2020, 44, 3838

Enhanced thermal stability and wettability of an electrospun fluorinated poly(aryl ether ketone) fibrous separator for lithium-ion batteries

Hai Li,[a] Feng Lin,[b] Hao Wang,[a] Haohan Wu,[a] Yunxu Yang,[a] Liang Yu,[a] Wei Liu *[a] and Dawei Luo*[ab]

Received 12th November 2019,
Accepted 24th January 2020

DOI: 10.1039/c9nj05656d

rsc.li/njc

To improve the safety and high performance of lithium-ion batteries (LIBs), a novel and heat-resistant fluorinated poly(aryl ether ketone) (FPAEK) compound was successfully synthesized and further fabricated as a nonwoven fibrous separator for LIBs *via* an electrospinning method. The morphology, thermal properties and electrochemical performances of the as-prepared electrospun FPAEK separators were characterized. The separator had no dimensional shrinkage at 150 °C for 1 h and no disintegration until reaching 500 °C. The electrospun FPAEK porous separators possessed much higher ionic conductivity (3.15 mS cm^{-1}) than that of a commercial polypropylene (PP) separator (0.66 mS cm^{-1}) due to their higher porosity and electrolyte uptake. The LIBs assembled with the electrospun fibrous separators exhibited higher discharge capacity (148.9 mA h g^{-1}) and longer cycle life (with 94.3% capacity retention after 250 cycles) than those assembled with the PP separator, with values of 139.5 mA h g^{-1} and 88.9%, respectively. The measurements demonstrated that electrospun FPAEK separators may be promising candidates for high-performance LIBs.

1. Introduction

Due to their high energy density, long cycle life and lack of memory effect, lithium-ion batteries (LIBs) have been widely applied to portable and dynamic devices such as mobile cell-phones and electric vehicles.[1–3] The separators are sandwiched between the anode and the cathode, allowing lithium ions (Li^+) to transfer quickly during the charge–discharge process and isolating direct contact of the two electrodes to avoid short circuits or even explosions.[4,5] Ideal LIB separators should possess high porosity, good wettability with liquid electrolytes, good electrolyte uptake, enhanced thermal and dimensional stability, low electrical resistance, small thickness, and excellent mechanical strength.[6] Currently, porous polyolefin separators containing polypropylene (PP), polyethylene (PE) and their derivative composite membranes are commonly adopted in commercial LIBs because of their good structure, superior mechanical strength to other materials and chemical stability.[7–10] However, commercial polyolefin separators still exhibit many disadvantages, such as low porosity, poor compatibility with liquid electrolytes and inferior thermal stability to other materials.[11–15] The melting points of the PE and PP separators are ~135 °C and ~165 °C, respectively.[16] The Celgard company has also focused its attention on PP/PE/PP trilayer blending separators with a thermal shutdown function. The sandwiched PE layer melts and occludes the microvoids at an elevated internal temperature of 130 °C, which prevents further increases in calorification, circuit destruction and even flame formation.[17,18] Porous polyolefin separators suffer from severe thermal shrinkage when the temperature exceeds 90 °C.[19]

To overcome the shortcomings (especially the poor thermal stability) of commercial polyolefin separators and to exploit novel high-performance LIB separators, extensive and significant studies have been performed in terms of fabrication techniques and the development of new types of polymer membranes,[20] for instance, stretching techniques, nonsolvent-induced phase separation, thermally induced phase separation, solvent evaporation-induced phase separation, surface grafting, blending, surface coating, electrospinning techniques and other methods.[21–25] To enhance the thermal stability and affinity with liquid electrolytes, many inorganic nanoparticles (*e.g.*, SiO_2, TiO_2, Al_2O_3, ZrO_2) have been used to modify porous LIB separators.[26–29] Guoqing Dong *et al.* employed titania (TiO_2) nanoshells to coat polyimide (PI) nanofiber membranes by a surface-alkaline-etching and *in situ* complexation–hydrolysis strategy, and the composite separator exhibited superior flame resistance, enhanced thermo-stability and improved wettability compared with an unmodified separator.[30] Simultaneously, an increasing number of polymers have been developed as porous membranes for LIBs, such as poly(acrylonitrile) (PAN), poly(ethylene oxide) (PEO), poly(methyl

[a] *Hoffmann Institute of Advanced Materials, Shenzhen Polytechnic, 7098 Liuxian Blvd, Nanshan District, Shenzhen 518055, China. E-mail: luodw@szpt.edu.cn, weiliu2018@szpt.edu.cn; Tel: +86 0755-26019983, +86 0755-26019310*

[b] *School of Applied Chemistry and Biological Technology, Shenzhen Polytechnic, 7098 Liuxian Blvd, Nanshan District, Shenzhen 518055, China*

methacrylate) (PMMA), poly(vinylidene fluoride) (PVDF), PI, and polyetherimide (PEI).[31–36] To some extent, these abovementioned membranes tend to swell due to the polar organic electrolyte liquid and do not simultaneously satisfy the mechanical strength and thermal stability requirements.[37,38]

Poly(aryl ether ketone) (PAEK) is a class of functional polymer materials with high thermal stability and enhanced chemical stability.[39,40] However, the PAEK polymer is not accessibly soluble in various polar organic solvents, which greatly affects its extensive and thorough applications.[41] Jing Li *et al.* prepared poly(ether ether ketone) (PEEK) with high ionic conductivity (1.68 mS cm^{-1}) and limited solubility by introducing a novel vapor-induced demixing method.[22] In this study, a novel, soluble and heat-resistant fluorinated poly(aryl ether ketone) (FPAEK) compound with abundant polar functional groups (–CO–, C–O–C, –F) and rigid molecular chain structures (containing benzene rings) was successfully synthesized and further fabricated into nonwoven nanofibrous separators *via* an electrospinning method. In addition, the electrospinning technique used in LIB separators results in high porosity, excellent compatibility with liquid electrolytes and a large specific surface area. The as-fabricated electrospun FPAEK membranes exhibited improved thermal stability compared with traditional membranes, high electrolyte uptake and high ionic conductivity. LIBs assembled with porous FPAEK displayed better electrochemical performances than those with commercial PP separators.

2. Experimental

2.1. Materials

Hexafluorobisphenol A, bisphenol A, bis(4-fluorophenyl)-methanone *N*-methyl-2-pyrrolidone (NMP) and *N*,*N*-dimethylacetamide (DMAc) were purchased from Shanghai Energy Chemical, Ltd, and potassium carbonate (K_2CO_3), dehydrated toluene, and methanol (Seebio Biomart, Ltd, Shanghai) were also used. The lithium iron phosphate ($LiFePO_4$) cathode, the acetylene black conductive additive, the PVDF binder and the lithium metal disc anode were from Shenzhen Kejing Star Technology Co., Ltd. An organic electrolyte solution composed of 1.0 M $LiPF_6$ in a mixed liquid of ethyl methyl carbonate (EMC), ethylene carbonate (EC) and dimethyl carbonate (DMC) (with a ratio of 1 : 1 : 1, v/v/v) was purchased from Guotai Huarong Company (China). A commercial PP separator (namely, a Celgard 2400 membrane) with a thickness of 25 μm was employed as a comparative LIB separator. Aluminum foil, hydrochloric acid (HCl) and other chemicals were used without further purification. The solvents DMAc and NMP were dried using 4 Å molecular sieves prior to use.

2.2. Synthesis of FPAEK

A series of FPAEK polymers with a range of polar functional groups were successfully prepared by nucleophilic aromatic substitution in one pot, and the detailed synthetic procedures are as follows: 3 mmol (0.6546 g) bis(4-fluorophenyl)methanone remained unchanged, but the amounts of hexafluorobisphenol A (X = 0, 0.25, 0.5, 0.75 mmol; corresponding mass = 0, 0.0841, 0.1681, 0.2522 g) and bisphenol A (Y = 3, 2.75, 2.5, 2.25 mmol; corresponding mass = 0.6849, 0.6278, 0.5707, 0.5137 g) were changed. Thus, where X represents the molar value of hexafluorobisphenol A and Y indicates the molar value of bisphenol A, the following relationship exists between X and Y: $X + Y = 3$ mmol. The corresponding molar amounts of the polymeric monomer hexafluorobisphenol A, bisphenol A and 3 mmol bis(4-fluorophenyl)methanone, 6 mmol (0.828 g) K_2CO_3 as an acid scavenger, 10 mL of DMAc as a dispersing agent and 10 mL of toluene as an azeotropic solvent were carefully added together in a 50 mL three-neck round-bottom flask equipped with a Dean–Stark trap and a condenser under a nitrogen atmosphere. The mixture was first stirred to create a uniform solution at room temperature and then heated at 142 °C (oil bath temperature) for 4 h to eliminate the water caused by the prereaction process *via* azeotropic distillation with anhydrous toluene. Subsequently, the temperature was elevated to 175 °C for 5 h to complete the condensation polymerization reaction and to distill the residual toluene. The obtained viscous fluorinated FPAEK polymers were slowly poured into a beaker containing 100 mL of distilled water and 100 mL of methanol to precipitate the polymers and remove the organic solvent. Finally, the polymer precipitates were submerged in a 1 mol L^{-1} HCl solution for 48 h and then washed three times with deionized water to thoroughly remove the residual inorganic salts. The fibrous FPAEK polymers were dried under vacuum at 120 °C for 24 h (yield: 96%). According to the molar ratio of hexafluorobisphenol A (X = 0, 0.25, 0.5 and 0.75 mmol), the series of FPAEK polymers were correspondingly named FPAEK-0, FPAEK-0.25, FPAEK-0.5 and FPAEK-0.75.

2.3. Fabrication of electrospun nonwoven fibrous FPAEK separators

A series of fibrous FPAEK separators including FPAEK-0, FPAEK-0.25, FPAEK-0.5 and FPAEK-0.75 were successfully fabricated into membranes by electrospinning. A homogenous polymer solution with a weight concentration of 10 wt% was prepared by dissolving the corresponding FPAEK polymers in anhydrous NMP solvent and loaded into a 10 mL plastic syringe pump with a stainless steel needle. During the electrospinning process, the plunger of the syringe containing the FPAEK solution was pushed with a flow rate of 0.5 mL h^{-1}, and a high voltage of 18 kV was applied to the metal needle during the whole electrospinning process. The collection distance between the rotating drum wrapped with aluminum foil and the spinneret was 20 cm, and the drum collector was rotated at 200 rpm. The thickness of the electrospun nonwoven fibrous separators was controlled to approximately 30 μm. Subsequently, all electrospun FPAEK nonwoven mats were dried in a vacuum oven at 60 °C for 24 h to remove residual solvent.

2.4. Electrode preparation

The cathode electrodes were fabricated in detail as follows: the dried active $LiFePO_4$ compound, the acetylene black conductive additive and the PVDF binder were mixed in a moderate NMP dispersing agent and stirred for 2 h. The mass ratio of $LiFePO_4$, PVDF and acetylene black was 8 : 1 : 1. The NMP-based slurry was coated on a flat aluminum current collector foil with a doctor blade. Then, the cathode electrodes were transferred into

a vacuum oven at 80 °C for 12 h to totally evaporate the solvent. The cathode electrode was further punched into a round disc with a diameter of 14 mm, and the active mass loading corresponded to a capacity of approximately 2.0 mA h cm^{-2}. The anode counterelectrode was lithium metal. The electrolyte liquid containing 1.0 M $LiPF_6$ in a mixture of EC, EMC and DMC (1 : 1 : 1, v/v/v) was purchased from Guotai Huarong Company (China) and used as received. A CR2032-type coin cell was assembled by sandwiching the electrospun FPAEK and commercial PP separator injected with an organic liquid electrolyte between the $LiFePO_4$ cathode electrode and the lithium metal anode. A conventional commercial PP separator (Celgard 2400) was also injected with the same amount of electrolyte and incorporated in an LIB for comparison. All the above cells were assembled in a dry argon-filled glove box.

2.5. Physical and electrochemical characterization

The chemical structures of the electrospun FPAEK separators were investigated by Fourier transform infrared (FTIR) spectroscopy using a Nicolet 6700 spectrometer with a wavenumber range of 4000–400 cm^{-1}.

The surface and cross-sectional morphologies of the LIB separators were observed by scanning electron microscopy (SEM, SU-70, Hitachi). Samples for studying the cross-sectional morphologies were fractured by liquid nitrogen. To enhance the surface conductivity, quality and resolution of the SEM images, all separators were sputtered with a platinum ion beam for 60 s before images were being captured.

The porosity (P) of the resultant LIB separators was determined by immersing them in n-butanol for 1 h at room temperature and performing the following calculation:

$$P\ (\%) = \frac{(m_{wet} - m_{dry})/\rho}{s \times d} \times 100\% \quad (1)$$

where P is the porosity of the separator, m_{wet} and m_{dry} are the weights of the wet separator and the dry separator, respectively, ρ is the density of the n-butanol solvent, and s and d are the area and thickness of the separator, respectively. All measured separators with a thickness of 25 μm were cut into a rectangular shape with a length of 2 cm and a width of 1 cm.

The electrolyte wettability of the separators was measured by an electrolyte droplet method in a glove box filled with argon. All dry separators were cut into round discs with a diameter of 16 mm, and then, 40 μL of the liquid electrolyte was added dropwise on the surface of the separator with a pipette. Moreover, the electrolyte wettability was also observed by the sessile drop method with a contact angle (CA) analyser (DSA100, Kruss) at room temperature. Notably, the droplet of the liquid electrolyte was limited to 5 μL to avoid gravitational distortion.

The electrolyte uptake (EU) of LIB separators is closely related to the Li ion conductivity, defined as the amount of electrolyte absorbed by the membrane, and is calculated by the following equation:

$$\mathrm{EU}\ (\%) = \frac{(W_{wet} - W_{dry})}{W_{dry}} \times 100\% \quad (2)$$

where EU (%) is the electrolyte uptake ratio and W_{dry} and W_{wet} are the weights before and after soaking the electrolyte liquid for 2 h, respectively. Similarly, all separators with an appropriate thickness of 25 μm were cut into a rectangular shape with a length of 2 cm and a width of 1 cm.

The thermal shrinkage of the separators was examined after each sample was deposited at 150 °C for 1 h. All separators were cut into circles with a 16 mm diameter, and the dimensional changes were photographed during the heat treatment.

In addition, the decomposition temperature and weight change of the LIB separators were analyzed by a Q50 thermogravimetric (TG) analyzer under a nitrogen flow of 40 mL min^{-1} from 50 °C to 800 °C at a heating rate of 10 °C min^{-1}.

The bulk impedance (R_b) of the LIB separators was measured by electrochemical impedance spectroscopy (EIS) using an electrochemical workstation CHI660E (Chenhua, China). The experiments were conducted in blocking cells, where the electrolyte-soaked membrane was sandwiched between two stainless steel electrodes. Impedance data were recorded in a frequency range from 1 Hz to 10^5 Hz with an AC amplitude of 10 mV under open-circuit potential conditions. The ionic conductivity was obtained according to the following equation:

$$\sigma = \frac{d}{R_b \times S} \quad (3)$$

where σ represents the ionic conductivity and R_b (Ω) is the bulk resistance. In this equation, d is the thickness of the separators, and S is recorded as the area of stainless steel. The area of the LIB separator was required to be larger than that of the stainless steel electrode.

The LIB performance parameters, including the charge–discharge, rate capacity and cycle life, were measured using a CR2032 coin half cell that was sandwiched with the electrolyte-soaked membrane between $LiFePO_4$ as the cathode and metallic lithium foil as the anode. The galvanostatic charge–discharge processes of the assembled coin cells were investigated at a current density of 0.5C within the voltage range of 2.7–4.2 V *versus* Li/Li^+ by using a CT2001A cell test instrument (LAND Electronic Co., Ltd, China). All tested half cells were assembled in a dry argon-filled glove box.

3. Results and discussion

3.1. Structures of FPAEK polymers

A series of FPAEK polymers were synthesized by a one-pot solution polycondensation method at a high temperature of 175 °C in a DMAc dispersing solvent, as shown in Scheme 1. To obtain a high molecular weight, the solution was very viscous and did not produce any precipitates during the experiment.

Fig. 1 shows the FTIR spectra of the FPAEK polymers obtained from the above polymeric reaction. The characteristic stretching vibration peak of the benzene ring was observed at 1589 cm^{-1}. The characteristic absorption peak of carbonyl (–CO–) groups was observed in the spectra at 1664 cm^{-1}. The in-plane bending vibration of C–H was found at 1497 cm^{-1}. The peaks at 1236 cm^{-1} and 1167 cm^{-1}, which corresponded to

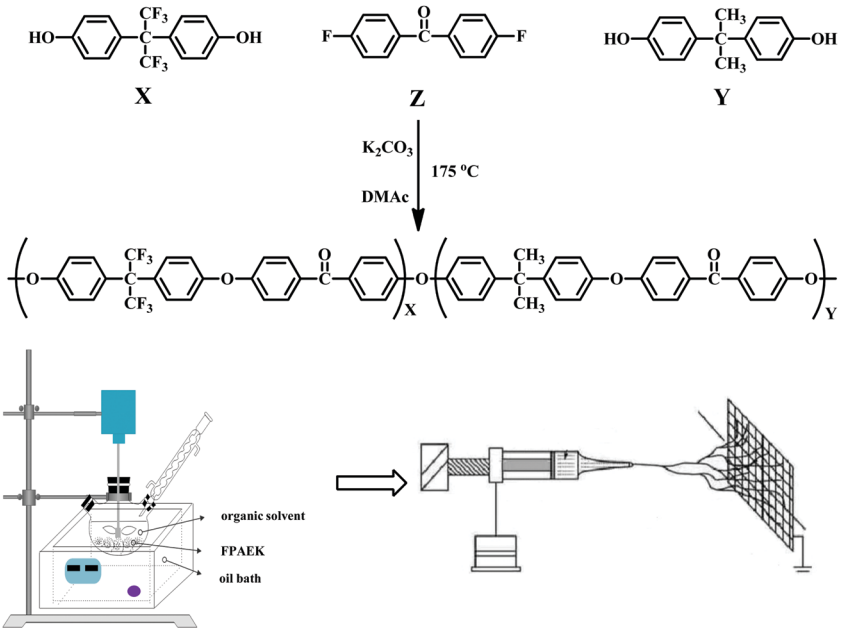

Scheme 1 Schematic of the preparation process of FPAEK.

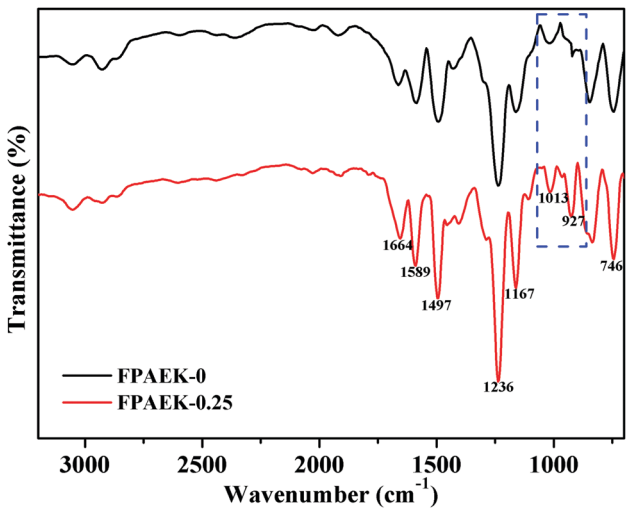

Fig. 1 FTIR spectra of FPAEK-0 and FPAEK-0.25 polymers.

the asymmetric and symmetric stretching vibrations of C–O–C bonds, indicated the successful synthesis of FPAEK. In addition, the main distinction between FPAEK-0 and FPAEK-0.25 is the presence of trifluoromethyl groups. C–F stretching vibrations were observed in the FPAEK-0.25 spectrum near 1000 cm^{-1}, as shown by the blue dashed rectangle, and no C–F chemical bonds were observed in the FPAEK-0 spectrum. From the results of the FTIR spectral characterization, we confirmed that the corresponding polymers were successfully synthesized.

3.2. Morphology, porosity, EU, and electrolyte wettability of the LIB separators

Fig. 2 depicts the pore structures and morphologies of the electrospun FPAEK-0, FPAEK-0.25, FPAEK-0.5 and FPAEK-0.75 LIB separators and the commercial PP separator, which were observed by SEM. Fig. 2(a) shows the surface morphology of a commercial microporous PP membrane, revealing a smooth surface and many elliptical pores with pore diameters in the range of 20–200 nm. Fig. 2(b) depicts the cross-sectional morphology of the PP separator, which exhibits peaks and valleys due to the application of a uniaxial stretching technology. Images (c), (e), (g) and (i) display the surface morphologies of the electrospun FPAEK-0, FPAEK-0.25, FPAEK-0.5 and FPAEK-0.75 separators, respectively. The images showed that these ether-based LIB separators are composed of countless randomly oriented fibers with fiber diameters ranging from hundreds of nanometers to several micrometers. The intersection of fibers formed interwoven nanopores and increased the mechanical strength of the separators, which was necessary for satisfying the requirements of LIBs. These twisted nanopores greatly improved the porosity and specific surface areas compared with conventional LIBs and had strong effects on preventing self-discharge and avoiding the internal short circuiting caused by particle migration between the anode and cathode or dendrite growth, thus enhancing the safety of LIBs.[12] As the microstructural images show, the FPAEK polymers were easily employed in the electrospinning technique, and as a result, no beads or agglomerates were attached to single nanofibers due to the excellent solubility that originated from the abundance of polar functional groups. In addition, as the fluorinated content ($-CF_3$) of the FPAEK separator was increased, thinner fibers were formed. Images (d), (f), (h) and (j) illustrate the cross-sectional morphologies of the electrospun FPAEK-0, FPAEK-0.25, FPAEK-0.5 and FPAEK-0.75 separators, respectively. The nanofibers were clearly cut, and the diameters of the cut fibers were consistent with the diameters measured from the surface images. Thus, the morphological structure of the FPAEK-based separators was characterized by high porosity,

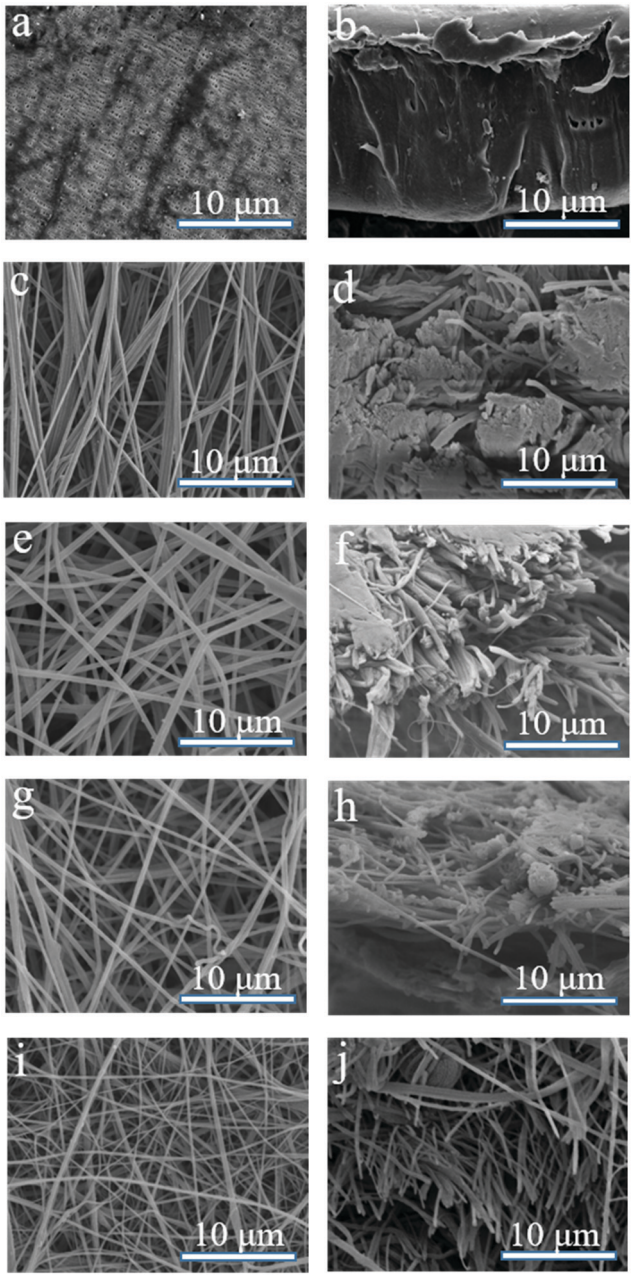

Fig. 2 SEM images of the surface morphologies of the PP (a), FPAEK-0 (c), FPAEK-0.25 (e), FPAEK-0.5 (g), and FPAEK-0.75 (i) separators and the cross-sectional morphologies of the PP (b), FPAEK-0 (d), FPAEK-0.25 (f), FPAEK-0.5 (h), and FPAEK-0.75 (j) separators.

which is beneficial for improving the uptake and wettability with the liquid electrolyte.

Porosity is a crucial parameter of LIB separators, as it can affect the lithium ion conductivity and electrochemical performance. If a separator has the necessary mechanical strength, then a high porosity is preferred for LIB separators because it can help in maintaining a sufficient amount of electrolyte and guarantee fast ion transport between two electrodes. Inversely, a low porosity leads to a high internal resistance. As shown in Table 1, the porosities of the electrospun nonwoven fibrous FPAEK-0, FPAEK-0.25, FPAEK-0.5 and FPAEK-0.75 separators were 92.7%, 89.4%, 87.6% and 84.5%, respectively. For the electrospun nanofibrous separators, the porosities decreased as the fiber diameters decreased. Generally, the electrospun FPAEK-based separators had much higher porosities than the commercial PP separator with a porosity of 40%.

The EUs of the electrospun fibrous separators and the commercial PP separator are shown in Table 1. Generally, a high porosity corresponds to a high EU. The EUs of the FPAEK-0, FPAEK-0.25, FPAEK-0.5, and FPAEK-0.75 separators and the commercial PP separator were 514%, 561%, 545%, 529% and 60%, respectively. The superior EUs of the electrospun FPAEK-based polymer separators compared with that of the PP separator could be attributed to the good affinity of the polymers with the electrolyte, the large specific surface area of the pore walls and the fully interconnected porous structure. However, the FPAEK-0 separator had the highest porosity but not the largest EU among the tested separators because the excessively large pore size caused slight leakage. Notably, the fluorinated separators had a greater EU due to the presence of trifluoromethyl groups in the molecular chain.

To obtain a low internal resistance in a cell, an LIB separator should be easily wetted by the liquid electrolyte so that it can absorb and retain a significant amount of electrolyte. As shown in Fig. 3, the wettability of the electrospun FPAEK-0, FPAEK-0.25, FPAEK-0.5 and FPAEK-0.75 separators and the commercial PP separator was investigated by quickly adding 40 μL of electrolyte dropwise on the surface of each separator. The PP separator was not totally wetted by the liquid electrolyte and generated a liquid droplet due to its poor ability to retain organic solvents and the hydrophobicity of its nonpolar structure. In contrast, the surfaces of all the electrospun fibrous membranes were quickly and completely wetted by the electrolyte, which is attributed to the interconnected three-dimensional and highly porous network

Table 1 Porosity (P), electrolyte uptake (EU) and ionic conductivity (σ) of the obtained electrospun FPAEK and commercial PP separators

	PP	FPAEK-0	FPAEK-0.25	FPAEK-0.5	FPAEK-0.75
P (%)	40	92.7	89.4	87.6	84.5
EU (%)	60	514	561	545	529
σ (mS cm^{-1})	0.66	2.73	3.15	2.94	2.81

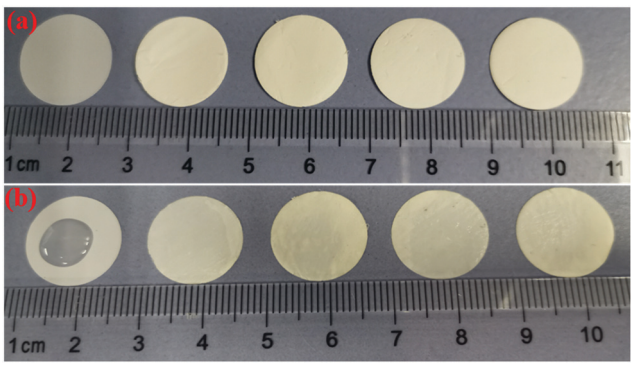

Fig. 3 Wettability images before (a) and after (b) adding the electrolyte dropwise on the surface of the separators: (left to right) PP, FPAEK-0, FPAEK-0.25, FPAEK-0.5, and FPAEK-0.75.

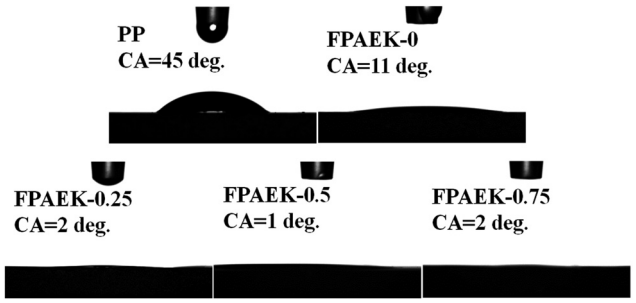

Fig. 4 CA images of PP, FPAEK-0, FPAEK-0.25, FPAEK-0.5, and FPAEK-0.75.

structures of these membranes with an ample number of polar functional groups. This property was beneficial for transporting lithium ions between the electrodes through the LIB separator. Better lithium ion transport can enhance the comprehensive electrochemical performance of the cells. In addition, Fig. 4 shows the images of the CA measurements for the LIB separators by immediately photographing the liquid electrolyte droplet after being added dropwise on the separators. Normally, a higher CA relates to a poorer affinity between the liquid electrolyte and the separator. As shown in Fig. 4, the CAs of FPAEK-0, FPAEK-0.25, FPAEK-0.5, and FPAEK-0.75 separators and the commercial PP separator were 11°, 2°, 1°, 2°, and 45°, respectively. This result further testifies that the electrospun non-woven nanofibrous FPAEK-based separators have much better wettability towards the liquid electrolyte than the commercial PP separator.

3.3. Thermal properties of the LIB separators

For safe operation of LIBs, another important property is the thermal dimensional stability of the separators. The separators should maintain dimensional stability at abnormally elevated temperatures to prevent thermal runaway between electrodes and avoid internal/external short circuits, expansion and even explosion. In the thermal shrinkage measurements of the series of electrospun FPAEK separators and the commercial PP separator, the dimensional changes were investigated at 150 °C over 1 h. Photographs of the FPAEK-0, FPAEK-0.25, FPAEK-0.5, FPAEK-0.75 and PP separators before and after heat treatment are shown in Fig. 5. The commercial PP separator showed extensive thermal shrinkage due to its intrinsically poor thermal stability, with a melting point of approximately 165 °C, which also easily caused a color change from white to semitransparent upon exposure to temperatures above 150 °C. Thus, the LIB assembled with the commercial PP separator may suffer from direct contact between the two electrodes at high temperatures. In stark contrast to the low thermal stability of the PP separator, all the electrospun fibrous FPAEK separators exhibited negligible thermal shrinkage and color changes because of their rigid molecular structures with high intrinsic melting temperatures.

The thermal properties of the LIB separators were further verified by TG analysis. Fig. 6 presents the TG curves of the electrospun porous FPAEK-0, FPAEK-0.25, FPAEK-0.5 and FPAEK-0.75 separators and the commercial PP separator. The thermal degradation of the commercial PP separator was found to start at 350 °C, whereas that of the superior ether-based FPAEK

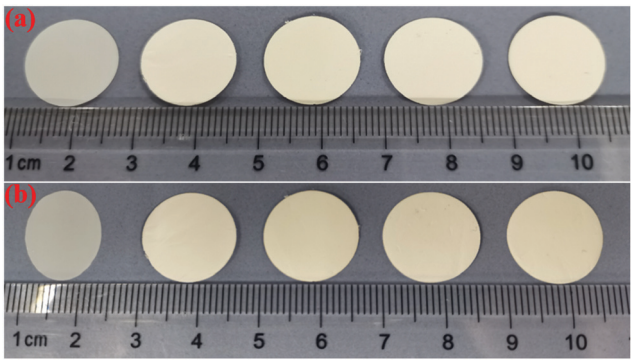

Fig. 5 Thermal shrinkage images of separators at 25 °C (a) and 150 °C for 1 h (b): (left to right) PP, FPAEK-0, FPAEK-0.25, FPAEK-0.5, and FPAEK-0.75.

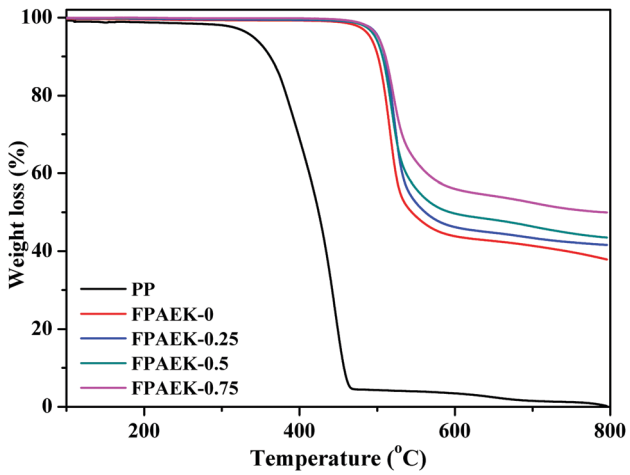

Fig. 6 TGA curves of the electrospun FPAEK-0, FPAEK-0.25, FPAEK-0.5 and FPAEK-0.75 separators and the commercial PP separator.

polymer separators was not observed until 500 °C. Compared to the commercial PP separator, all the electrospun fibrous separators showed better thermal stabilities, which were attributed to their rigid structures.

3.4. Electrochemical properties of the FPAEK-0, FPAEK-0.25, FPAEK-0.5, FPAEK-0.75 and PP separators

Fig. 7 displays the Nyquist curves of the symmetric cells (*i.e.*, stainless steel/electrolyte-soaked separator/stainless steel) prepared from the electrospun porous FPAEK-0, FPAEK-0.25, FPAEK-0.5, and FPAEK-0.75 separators and the commercial PP separator; the curves were measured by EIS at 25 °C. The conductivity of the corresponding separator was calculated using the bulk resistance (R_b) of the membrane, which was determined from the intercept of the extrapolated plot at the high-frequency end of the real axis. The electrospun fibrous nonwoven PAEK-0, FPAEK-0.25, FPAEK-0.5 and FPAEK-0.75 separators exhibited lower bulk resistances than the commercial PP separator. The bulk resistances of the porous FPAEK-0, FPAEK-0.25, FPAEK-0.5, FPAEK-0.75 and PP separators were 2.65, 2.02, 2.24, 2.39 and 2.91 Ω, respectively. By considering the area of the stainless steel blocking electrodes and the thickness of the LIB separators, the ionic conductivities were calculated to be

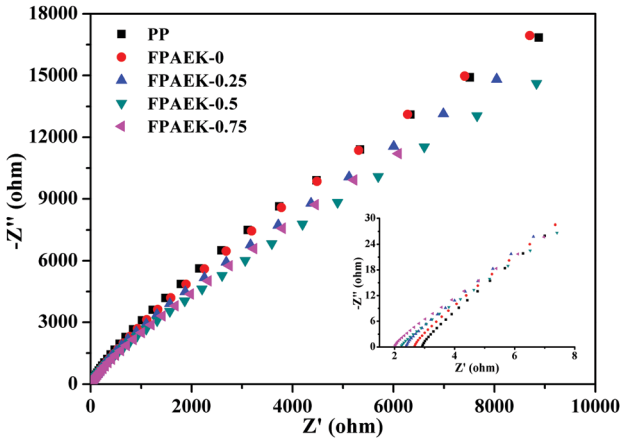

Fig. 7 Nyquist plots of electrolyte-soaked FPAEK-0, FPAEK-0.25, FPAEK-0.5, FPAEK-0.75 and commercial PP separators.

2.73, 3.15, 2.94 and 2.81 mS cm^{-1} for FPAEK-0, FPAEK-0.25, FPAEK-0.5 and FPAEK-0.75, respectively, which were much higher than that of the commercial PP separator with a value of 0.66 mS cm^{-1}, as shown in Table 1. This high ionic conductivity was consistent with the high EU of the electrospun separators. Ion transport increases with the amount of electrolyte stored in the porous separators, which accordingly enhances the lithium ion conductivity of an electrolyte-soaked separator. In addition, a higher porosity can provide more channels for lithium ion transport and decrease the resistance. The FPAEK-0.25 separator with few fluorinated groups had the greatest ionic conductivity among the tested separators due to the improved compatibility with the organic liquid electrolyte, which resulted from the comprehensive effects of the EU and porosity; thus, the EU may be the main influencing factor. As the fluorinated group content increased, the FPAEK polymers swelled in the electrolyte to some extent and impaired the corrosion resistance.

3.5. Performances of the cells assembled with FPAEK-0, FPAEK-0.25, FPAEK-0.5, FPAEK-0.75 and PP separators

To evaluate the long-term stabilities of the separators, the cycle lives of cells assembled with the electrospun porous FPAEK-0, FPAEK-0.25, FPAEK-0.5, and FPAEK-0.75 separators and the commercial PP separator were tested within a voltage range from 2.7 V to 4.2 V with a constant charge current density of 0.5C at 25 °C. Fig. 8(a) displays the cycling performance of the cells assembled with different separators over 250 charge–discharge cycles. Within the first 20 cycles, the discharge capacity of the cell assembled with the commercial PP separator increased from 136.6 mA h g^{-1} to 139.5 mA h g^{-1}. As more cycles were completed, the PP separator became completely wetted, and the active substance was gradually activated. Then, the discharge capacity became stable and decreased slowly with a final capacity retention of 88.9% after 250 charge and discharge cycles. The LIBs assembled with the electrospun porous FPAEK-0, FPAEK-0.25, FPAEK-0.5 and FPAEK-0.75 separators exhibited larger discharge capacities than the Celgard 2400 membrane, which was attributed to their much higher porosities and better affinities for the liquid electrolyte. The LIBs with electrospun separators showed more stable discharge capacities during the 250 cycles than those of LIBs with the PP separator and possessed a capacity retention ratio of approximately 94.3% after 250 cycles due to the sufficient wettability of the electrospun separators by the electrolyte. The LIB assembled with the electrospun FPAEK-0.25 separator possessed the highest discharge capacity of the tested separators, which corresponded to its best ionic conductivity. The cycle life test implied that the electrospun FPAEK-0, FPAEK-0.25, FPAEK-0.5 and FPAEK-0.75 separators had adequate chemical and morphological stabilities to function as LIB separators.

The galvanostatic charge and discharge curves of the 1st, 50th, 100th, 150th, 200th and 250th cycles at a constant current of 0.5C and room temperature of a coin half cell assembled with the electrospun FPAEK-0, FPAEK-0.25, FPAEK-0.5 and FPAEK-0.75 separators and the commercial PP separator were recorded, and the results are shown in Fig. 8(b) and Fig. 9. The charge/discharge curves for all the cells had stable plateaus and good reproducibility, even after 250 cycles, while the cell that contained the electrospun porous FPAEK-0.25 exhibited the highest capacity due to its high porosity, good compatibility with the electrolyte and the highest EU among the tested cells.

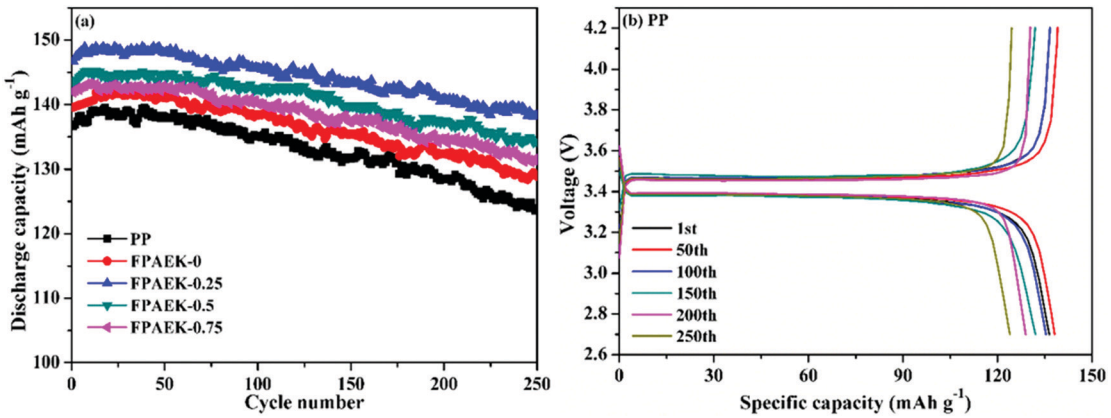

Fig. 8 Discharge cycling performance (a) of the cells at 25 °C and a rate of 0.5C; (b) charge–discharge curves for the LIBs assembled with commercial PP separators.

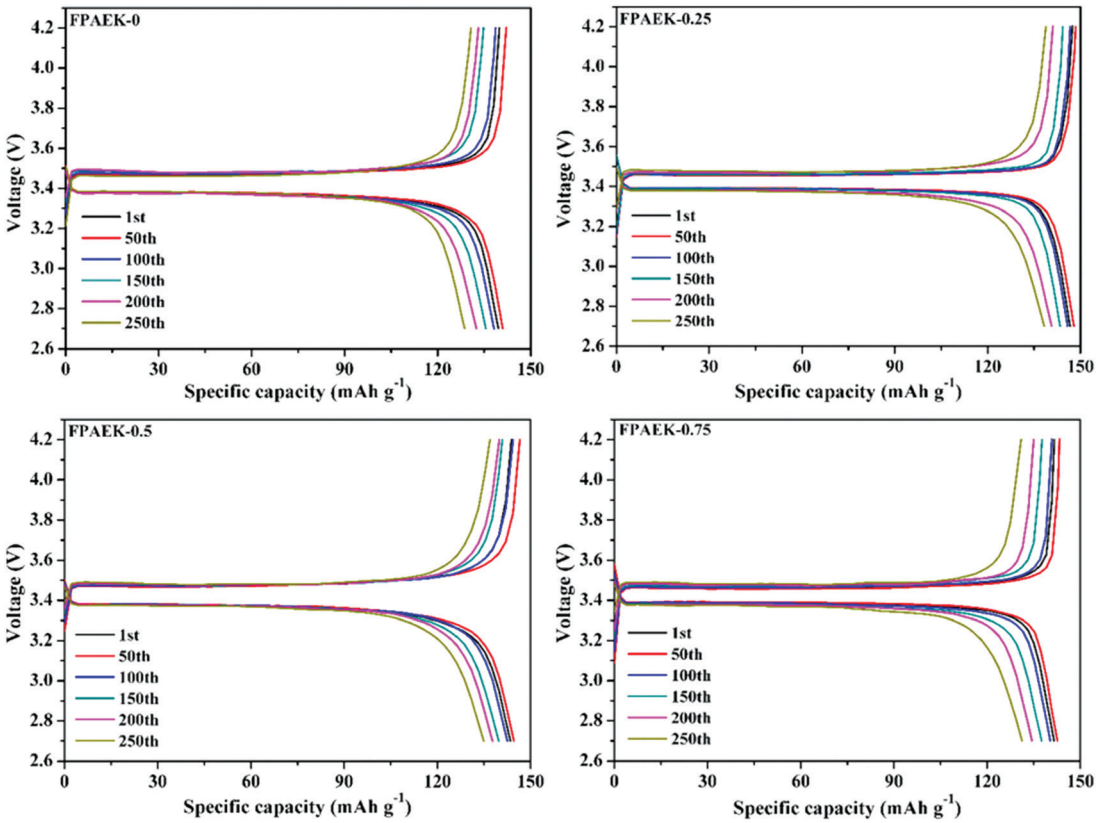

Fig. 9 Charge–discharge curves for the LIBs assembled with the electrospun FPAEK-0, FPAEK-0.25, FPAEK-0.5, and FPAEK-0.75 separators.

After sufficient wetting of the LIB separator and activation of the $LiFePO_4$ cathode, the cell capacity declined gradually with an increasing number of charge–discharge cycles (*i.e.*, 1st, 50th, 100th, 150th, 200th, and 250th cycles). The initial discharge capacities were 139.6, 146.7, 143.3, 141.9 and 136.6 mA h g^{-1} for the electrospun porous FPAEK-0, FPAEK-0.25, FPAEK-0.5 and FPAEK-0.75 separators and the commercial PP separator, respectively. The change in the cell discharge capacity was consistent with the trend in the ionic conductivity of each separator.

4. Conclusions

In our work, a series of heat-resistant FPAEK polymers (including FPAEK-0, FPAEK-0.25, FPAEK-0.5 and FPAEK-0.75) were successfully synthesized by controlling the content of the reactive monomer hexafluorobisphenol A and further fabricated into porous fibrous separators *via* the electrospinning technique. Compared to the commercial PP separator, all the electrospun PAEK-based separators demonstrated much higher porosities and EUs. The ionic conductivities of the fibrous FPAEK-0, FPAEK-0.25, FPAEK-0.5, and FPAEK-0.75 separators and the commercial PP separator were 2.73, 3.15, 2.94, 2.81 and 0.66 mS cm^{-1}, respectively, which followed the same trend as the corresponding EUs. More importantly, the cells assembled with electrospun fibrous separators exhibited higher discharge capacities and more stable discharge plateaus than those assembled from the commercial PP separator, which was related to the much higher porosity, ionic conductivity and thermal stability of the PAEK-based separators. In particular, the FPAEK separators had the best comprehensive performance among the three kinds of LIB separators as a result of their outstanding physical and chemical properties and were highly competitive separators for application in LIBs.

Conflicts of interest

There are no conflicts to declare.

Acknowledgements

We gratefully acknowledge the financial support from the Natural Science Foundation of Guangdong Province (2018A030313371), National Natural Science Foundation of China (21901167), Shenzhen Science and Technology Innovation Commission (JCYJ20180307102051326).

References

1 R. Gonçalves, T. Marques-Almeida, D. Miranda, M. M. Silva, V. F. Cardoso, C. M. Costa and S. Lanceros-Méndez, *Energy Storage Materials*, 2019, **21**, 124–135.
2 G. Zeng, J. Zhao, C. Feng, D. Chen, Y. Meng, B. Boateng, N. Lu and W. He, *ACS Appl. Mater. Interfaces*, 2019, **11**, 26402–26411.

3 X. Zhou, Z. Dai, S. Liu, J. Bao and Y. G. Guo, *Adv. Mater.*, 2014, **26**, 3943–3949.
4 X. Ge, S. Liu, M. Qiao, Y. Du, Y. Li, J. Bao and X. Zhou, *Angew. Chem.*, 2019, **58**, 14578–14583.
5 H. Li, L. Li, S. Zheng, X. Wang and Z. Ma, *Materials*, 2019, **12**, 1–11.
6 W. Gong, J. Gu, S. Ruan and C. Shen, *Polym. Bull.*, 2019, **76**, 5451–5462.
7 L. Fu, L. Shi, Z. Wang, J. Zhu, Y. Zhao and S. Yuan, *Res. Chem. Intermed.*, 2019, **45**, 4959–4973.
8 W. Gong, X. Wang, Z. Li, J. Gu, S. Ruan and C. Shen, *High Perform. Polym.*, 2018, **31**, 948–958.
9 H. Li, D. Wu, J. Wu, L. Y. Dong, Y. J. Zhu and X. Hu, *Adv. Mater.*, 2017, **29**, 1–11.
10 C. Zhang, H.-Q. Liang, J.-K. Pi, G.-P. Wu and Z.-K. Xu, *Chin. J. Polym. Sci.*, 2019, **37**, 1015–1022.
11 D. Parikh, T. Christensen, C.-T. Hsieh and J. Li, *J. Electrochem. Soc.*, 2019, **166**, A3377–A3383.
12 Y. Wang, C. Yin, Z. Song, Q. Wang, Y. Lan, J. Luo, L. Bo, Z. Yue, F. Sun and X. Li, *Materials*, 2019, **12**, 1–13.
13 C. Zhang, L. Shen, J. Shen, F. Liu, G. Chen, R. Tao, S. Ma, Y. Peng and Y. Lu, *Adv. Mater.*, 2019, **31**, 1–8.
14 H. Zheng, Z. Wang, L. Shi, Y. Zhao and S. Yuan, *J. Colloid Interface Sci.*, 2019, **554**, 29–38.
15 C. Zhu, J. Zhang, J. Xu, X. Yin, J. Wu, S. Chen, Z. Zhu, L. Wang and H. Wang, *J. Membr. Sci.*, 2019, **588**, 117169.
16 Z. Wang, Y. Xie, C. Xu, S. Shi, L. Wang, G. Zhang, X. Wang, L. Zhu and D. Xu, *J. Solid State Electrochem.*, 2018, **23**, 269–276.
17 M. Chen, J. Mei and H. Liu, *Int. J. Energy Res.*, 2019, **44**, 218–228.
18 C. Feng, X. Wang, G. Zeng, D. Chen, W. Lv, Y. Han, X. Jian, S. X. Dou, J. Xiong and W. He, *Phys. Status Solidi RRL*, 2019, **14**, 1–8.
19 G. Zhong, Y. Wang, C. Wang, Z. Wang, S. Guo, L. Wang, X. Liang and H. Xiang, *Ionics*, 2018, **25**, 2677–2684.
20 Q. Song, A. Li, L. Shi, C. Qian, T. G. Feric, Y. Fu, H. Zhang, Z. Li, P. Wang, Z. Li, H. Zhai, X. Wang, M. Dontigny, K. Zaghib, A.-H. Park, K. Myers, X. Chuan and Y. Yang, *Energy Storage Materials*, 2019, **22**, 48–56.
21 L. Ding, R. Xu, L. Pu, F. Yang, T. Wu and M. Xiang, *Mater. Des.*, 2019, **179**, 107880.
22 J. Li, X. Niu, J. Song, Y. Li, X. Li, W. Hao, J. Fang and T. He, *J. Membr. Sci.*, 2019, **577**, 1–11.
23 M. Waqas, S. Ali, C. Feng, D. Chen, J. Han and W. He, *Small*, 2019, **15**, e1901689.
24 S. Wu, J. Ning, F. Jiang, J. Shi and F. Huang, *ACS Omega*, 2019, **4**, 16309–16317.
25 H. Zhao, N. Deng, J. Yan, W. Kang, J. Ju, L. Wang, Z. Li and B. Cheng, *Chem. Eng. J.*, 2019, **356**, 11–21.
26 H. Cai, G. Yang, Z. Meng, X. Yin, H. Zhang and H. Tang, *Polymers*, 2019, **11**, 1–13.
27 S.-J. Tan, X.-X. Zeng, Q. Ma, X.-W. Wu and Y.-G. Guo, *Electrochem. Energy Rev.*, 2018, **1**, 113–138.
28 K. Zhang, W. Xiao, J. Liu and C. Yan, *J. Solid State Electrochem.*, 2019, **23**, 2853–2862.
29 X. Zhou, L. J. Wan and Y. G. Guo, *Small*, 2013, **9**, 2684–2688.
30 G. Dong, B. Liu, G. Sun, G. Tian, S. Qi and D. Wu, *J. Membr. Sci.*, 2019, **577**, 249–257.
31 Z. Liang, Y. Zhao and Y. Li, *Energies*, 2019, **12**, 3391.
32 J. Liu, M. Liu, C. He, J. Li, Q. Li, C. Wang and Y. Xi, *Ionics*, 2019, **25**, 5201–5211.
33 J. Mohanta, O. H. Kwon, J. H. Choi, Y. M. Yun, J. K. Kim and S. M. Jeong, *Nanomaterials*, 2019, **9**, 1–13.
34 X. Shen, Z. Li, N. Deng, W. Kang, J. Fan and Y. Liu, *Electrochim. Acta*, 2019, **318**, 801–808.
35 L. Wang, F. Liu, W. Shao, S. Cui, Y. Zhao, Y. Zhou and J. He, *Compos. Commun.*, 2019, **16**, 150–157.
36 H. Zhang, J. Zhang, J. Ma, G. Xu, T. Dong and G. Cui, *Electrochem. Energy Rev.*, 2019, **2**, 128–148.
37 Z. Hao, C. Wu, Q. Zhang, J. Liu and H. Wang, *Int. J. Energy Res.*, 2019, **43**, 8049–8056.
38 D. Li, H. Xu, Y. Liu, Y. Jiang, F. Li and B. Xue, *Ionics*, 2019, **25**, 5341–5351.
39 D. Li, D. Shi, K. Feng, X. Li and H. Zhang, *J. Membr. Sci.*, 2017, **530**, 125–131.
40 Y. Li, Q. Li and Z. Tan, *J. Power Sources*, 2019, **443**, 227262.
41 H. Li, B. Zhang, B. Lin, Y. Yang, Y. Zhao and L. Wang, *J. Electrochem. Soc.*, 2018, **165**, A939–A946.

